

MEMS Shear Stress Sensor for Hypersonic Aeropropulsion Test and Evaluation

Nicholas Tiliakos¹ and George Papadopoulos²
Advanced Concepts Group, Technology Development Department
ATK GASL
Ronkonkoma, N.Y., 11779

Vijay Modi³, Andrew O'Grady⁴, Matthew McCarthy⁵
Dept. of Mechanical Engineering, Columbia University
New York, NY 10027

Luc Frechette⁶, Jean-Philippe Desbiens⁷, Ronan Larger⁸
University of Sherbrooke
Sherbrooke, Quebec, CAN

Abstract

An integral part of assessing an aircraft's performance is accurate determination of its viscous drag and combustion efficiency, both of which are functions of surface shear stress forces. The measurement of shear stress is important for: improving the performance of aerospace vehicles by assessing and reducing viscous drag; understanding and characterizing laminar to turbulent boundary layer transition and separated flows and the emerging field of active flow control. Wall shear stress is a measurement that is not readily made and has been relatively absent from wind tunnel testing. In this paper we present our research, development and testing effort of a MEMS based shear stress sensor can be used to directly measure the shear stress on ground based articles tested in hypersonic aeropropulsion tunnels, and eventually on flight-test articles. The paper will describe our efforts over the past year and half to design, develop, fabricate and test a silicon carbide (SiC) MEMS shear stress sensor for hypersonic aeropropulsion test and evaluation applications.

¹ Senior Scientist, Advanced Concepts Group, ATK GASL/ Adjunct Professor, ME Dept., Columbia University, NYC; Nicholas.Tiliakos@ATK.com

² Manager, Advanced Concepts Group, ATK GASL; George.Papadopoulos@ATK.com

³ Professor, ME Dept, Columbia University

⁴ Ph.D. Candidate, ME Dept. Columbia University

⁵ Ph.D. Candidate, ME Dept. Columbia University

⁶ Assistant Professor, University of Sherbrooke

⁷ Research Associate, University of Sherbrooke

⁸ Ph.D. Candidate, University of Sherbrooke

I. Introduction

The goal of this work is to develop a MEMS wall shear stress sensor for application in high-speed aeropropulsion wind tunnels and other “harsh“ environments (eg. combustors, rocket nozzles, airfoils), and eventually for flight test applications. A measurement that is not readily made and has been absent from aeropropulsion/hypersonic wind tunnel testing is wall shear stress. This paper describes research performed by ATK GASL, in collaboration with Columbia University and the University of Sherbrooke, on the development of a MEMS based direct shear stress sensor designed for the unique environment and shear stress levels found in such harsh aeropropulsion applications.

MEMS (MicroElectroMechanical Systems) is an enabling technology that utilizes surface and bulk micromachining methods, an extension of integrated circuit technology, to create structures on the order of microns. Some of the benefits of using MEMS include: (1) batch fabrication leads to cost reduction; (2) small size allows for minimal disturbance, weight savings and integration of sensor, actuator and “smart” electronics in an area the size of a human pupil; and (3) very low power requirements.

Obtaining direct shear stress measurements along, for example, the combustor wall of an aerospace vehicle, will: (1) allow for direct measurement of vehicle component drag; (2) may contribute to more accurate combustor performance and thermal load assessment (using Reynolds Analogy); (3) allow for calibration of computer code shear stress calculations; (4) help identify when and where flow separation and boundary layer transition occurs in the engine flow path.

With the shear stress sensor technology currently available it is difficult, if not impossible to meet the following competing requirements with a single sensor measurement technique: (1) obtaining shear stress measurements over large portions of the wind tunnel aeropropulsion model; (2) utilizing miniature shear stress sensors to obtain spatial resolution; (3) measuring fluctuating shear-stress, especially important in turbulent boundary layers; and (4) surviving harsh/hypersonic environments characteristic of aerothermal applications.

The scope of this effort is to design, fabricate and test a MEMS shear stress sensor for aeropropulsion applications, with initial benchtop and cold-flow testing conducted at Columbia University and ATK GASL with subsequent testing in the hypersonic aeropropulsion tunnels at ATK GASL. In parallel, technology development will occur in the areas of (1) silicon carbide deep etching techniques; (2) high temperature electrical connections; and (3) sensor packaging. Eventually, our goal is to be able to implement an array comprised of several MEMS shear stress sensors in the harsh environment of a propulsion device (inlet, combustor, nozzle, etc).

ATK GASL, Columbia University and the University of Sherbrooke have teamed together, over the past several years, on developing a MEMS based shear stress sensor.¹ This paper will discuss our progress in the design, fabrication and testing of two generations of MEMS SiC sensors, i.e. the breadboard (Phase I) and brassboard (Phase II) series of sensors, part of a three phase effort funded by the Test Resource Management Center (TRMC) Test and Evaluation/Science and Technology

(T&E/S&T) Program, though Arnold Engineering Development Center (AEDC).

II. MEMS Based Shear Stress Sensors

Shear stress sensors use either direct or indirect methods for shear stress detection.² In the direct method the tangential force, i.e. shear, acts on a surface floating balance, thus giving the shear stress directly.^{3,4} The deflection of the floating element is then proportional to the shear.

For the indirect shear stress measuring methods, the shear stress is obtained by making measurements that are related to shear stress through some physical principle, eg. heat transfer. Some indirect measuring devices include: Preston tubes⁵, Stanton tubes⁶, and hot-wire/hot-film surface mounted sensors.⁷ Flow sensors based on heat transfer methods have a common problem in that the heat loss to the wall or substrate beneath the sensor limits their performance.

The micromachined devices discussed in Refs [8-10] measured shear stress levels in the range that are far below the range encountered in the supersonic/hypersonic flowfield environments typical of hypersonic aeropropulsion wind tunnels and are not well suited for harsh environment applications. Wide dynamic range of shear stress and harsh environment applications for hypersonic test and evaluation efforts are the primary reasons for developing the MEMS shear stress sensor discussed in this paper.

III. Breadboard Sensor Design

A. Requirements

A MEMS shear stress sensor prototype (Phase III) design shall meet the following requirements:

- High temperature survivability
- Chemically non-reacting

- Non-intrusive
- Wide dynamic range
- High frequency response

The high temperature survivability requires that the sensor be fabricated out of Silicon Carbide (SiC). The fact that the sensor was MEMS based, with dimensions $\sim O(\mu\text{m})$, with very low mass, $\sim O(\text{mg})$, and was installed flush mounted ensured that it allowed for a high frequency response and that it was non-intrusive. In addition, the wide dynamic range (10-10,000 Pa) requirement will be satisfied by closed feedback loop electronics.

Though the breadboard sensor was designed for a wide shear stress range and a harsh environment, during Phase I research it was cold flow tested in a fully developed, turbulent flow, duct that provided a maximum shear stress of 300 Pa. The breadboard sensor was designed with the requirements presented and discussed in Ref [1].

B. Breadboard Sensor Theory of Operation/Design

The overall sensor design process consisted of defining a sensor geometry which provided a measurable output at the lowest level of shear, sufficient electrostatic force feedback to maintain the shuttle in a neutral position at the highest level of shear, all within the fabrication constraints imposed by the microfabrication technology, available circuitry, and physical constraints. The SiC surface micromachining process used set the thickness of each layer forming the device, but there was complete flexibility for the in-plane geometry, with minimum feature size of 2 microns ($1/10,000^{\text{th}}$ inch).

The sensor operation consisted of directly monitoring the shear force applied by the flow on a freely suspended sensing element flush with the wall. The sensor was fabricated using MEMS microfabrication techniques and

integrated the exposed sensing element, mechanical compliance, capacitive sensing, and electrostatic force feedback on a chip, as shown in Figure 1. Each chip contained 12 MEMS shear stress sensors, with a total of six chips. Each sensor had '-', '+', and ground Ni contact pads (on the front sides, exposed to the flow) used to transmit sensor voltage signals to the data system and discussed in detail in Ref [1].

The breadboard sensor configuration and its operating principles are illustrated in Figure 1. A lateral force is applied on the sensing element proportional to the local shear stress. This force is transmitted to a free-floating shuttle supported on springs. The springs consist of pairs of folded cantilever beams at each end of the shuttle. When the shuttle translates, the gaps between electrodes attached to the shuttle and stationary electrodes varies, leading to a change of electrical capacitance (δC) between the two structures. This change of capacitance was measured with external circuitry (MS3110)¹¹ and converted into a voltage signal, V_{sensed} , Figure 1.

To increase the range of shear applied before the movable shuttle contacts the stationary structures, an electrostatic counterforce is applied to the shuttle by applying a potential difference, V_{control} , between the stationary and movable electrodes, Figure 1. The device is then maintained in the central position (i.e. "null" condition) and the actuation voltage becomes the output quantity, via closed loop feedback control circuitry. This electric force feedback is what enables the sensor to measure a relatively wide range of shear stress.

In defining the breadboard sensor geometry, the springs were implemented as cantilever beams and the capacitance change was

determined by the parallel plate capacitance between the stationary and movable electrodes. Since commercially available differential capacitance circuitry allows measurements on the order of 1fF, the lowest shear level must provide sufficient deflection and a measurable change of capacitance. This suggests thin clearances between electrodes, flexible springs, and a large number of electrodes, N_f , (proportional to capacitance area). At high shear levels, a maximum voltage of 100 V was allowed between the stationary and movable electrodes in order to counteract the shear force, and maintain the shuttle centered (i.e. null position). Any voltage $\gg 100$ V may lead to a voltage breakdown of the air in the electrode gaps.¹² The design objective was to minimize the number of electrodes N_f , hence minimizing the device size, while achieving the desired shear stress range of 10-10,000 Pa. This design analysis was discussed in detail in Ref [1].

Given the requirements and constraints, various designs were possible. Table 1 summarizes the nominal breadboard design ('A') as well as six other alternative designs ('B'-'G'), which relax some of the specifications and constraints. All the sensors include reference sensors that are not free to move under the shear flow. These reference sensors are used to assess the impact of shock or thermal expansion on the sensor operation and allow the measurement from the actual sensor to be corrected.

C. Sensor Fabrication

Since the MEMS shear stress sensor will be directly exposed to harsh aeropropulsion environments, its fabrication must be based on materials and operating principles that maintain sensor functionality at elevated temperatures and maintain sensor chemical stability. Silicon carbide appears as a material

of choice, especially given the recent development of SiC MEMS microfabrication techniques at Case Western Reserve University (CWRU)¹³ and Flx Micro.¹⁴

The following steps summarize the SiC MuSiC¹⁴ micro-fabrication and etching processes used for the breadboard sensor fabrication:

1. SiC layers, Figure 2, are created via micromolding, i.e. a sacrificial mold material (oxide or polysilicon) is first deposited.
2. A reverse pattern is etched into mold material.
3. SiC film is deposited to fill the mold.
4. Chemical-mechanical polishing (CMP) is performed to planarize SiC mold.
5. Etching Steps (to release structures):
 - a. PhotoResist and Nickel Etch (Optional)
 - b. HF - Etches SiO₂ (Releases SiC-3, SiC2-3 layers)
 - c. KOH - Etches Poly-Silicon (Releases SiC-2 layer)
 - d. HF - Etches SiO₂ (Releases SiC-2, SiC-1 layers)

The resulting films contain the desired pattern in SiC, surrounded by the sacrificial layer, which is then removed via chemical etchants.

The various layers that comprise the MEMS shear stress sensor are depicted in Figure 2. The SiC-3 layer is used for free-standing structures and contains the sensing element. This layer is a 1.5 μm thick SiC layer. Next is the via ('V') layer, which provides the through-hole for the sensing element anchor and is 0.75 μm thick. The SiC-2 layer contains the shuttle, stationary electrodes, shuttle fingers and the spring and is used for free-standing structures. The SiC-1 layer serves as the anchor layer for the stationary electrode anchor pads, anchoring the upper

SiC layers; it cannot be used to make free-standing structures. Finally, the SiC-0 layer serves as the supporting layer for SiC-1 and the electrical connection (+/-) paths to the stationary electrodes. The sacrificial mold layer SiO₂ is everywhere, except the SiC-2 layer which is surrounded by poly-Si. The SiC-0, SiC-1 and SiC-2 layers are created via micro molding as opposed to traditional DRIE (Deep Reactive Ion Etching).

D. Sensor Packaging

Most of the critical components of the breadboard sensor were protected from the environment by the top SiC layer, which covered the entire device surrounding the sensing element. Holes and clearances were less than 5 microns, which prevented typical size dust particles from entering the device.

One of the main packaging requirements for the breadboard sensor was to have it packaged in a structure that can be readily installed, flush to the wind tunnel (or test article) wall and directly exposed to the flow. Electrical connections to the sensor components for the breadboard sensor were accomplished through the use of gold wirebonds, which connected the sensor's Ni contact pad, to a chip carrier (LCC) terminal, and then to a socket mount, as shown in Figure 3. The socket mount had pin connections that can then be mated to a pin connector cable, which provided signal transmission to a data acquisition computer.

The overall sensor package/mount design allowed for the MEMS shear stress sensor to be situated inside the 0.25" x 0.25" chip carrier cavity (LCC), on top of a 0.020" thick plastic shim, ensuring the sensor is flush with the top of the LCC. The sensor was glued to the bottom of the chip carrier cavity using photoresist (PR). A "dummy" chip, completely covered with photoresist (PR), was tested in the tunnel to ascertain if the

photoresist “flowed” at all during high subsonic ($M \sim 0.7-0.8$) flow. Tunnel tests were conducted at various air mass flow rates and pre-test and post test boroscope photos of the dummy chip showed that the PR remained intact.

Wirebonding electrically connected the sensor to the chip carrier, which contained 28 terminal pads; only 18 were required for the six sensors on each MEMS chip, (Chips ‘1’-‘6’). Photoresist was used to provide strength and adhesion to the base of the wirebond, as well as to fill in the trench around the MEMS chip. All the wirebonds were inspected under a microscope to ensure proper application at the contact points. Electrical continuity checkouts (before and after tests) were also made to verify electrical connectivity from the sensor contact pad to the socket mount.

The MEMS chip plus chip carrier combination was then placed inside a modified COTS (Commercial Off-the-Shelf) “live-bug” socket mount, Figure 3, which was then readily installed inside a support tray and into the wind tunnel wall for calibration tests.

E. Electrical Characterization Tests

For electrostatic actuation tests, the MEMS chip, chip carrier plus socket mount combination was installed in a specifically designed set-up for testing the sensor with varying bias voltages (V_{bias}) to determine: (a) whether the sensor is completely released; and (b) the sensor’s electrical characteristics, i.e. resistance, capacitance measurements, as a function of V_{bias} . Each chip contained multiple sensors (labeled ‘A’-‘G’, Table 1, with a total of six chips. A probe station was used to determine the sensor’s C-V (capacitance as a function of voltage) characteristic.

Initial device inspection and electrical characterization was performed in the CEPSR (Center for Engineering and Physical Science Research) cleanroom at Columbia University in order to validate the dimensions and basic functionality of the sensor. Breadboard electronics with off-the-shelf integrated circuitry for differential capacitance measurement was used (MS3110 board).¹¹

Prior to the electrostatic actuation testing, a performance analysis for the breadboard sensors on Chips 4 and 6 was conducted (these chips contained sensors with the highest probability of operation based on their low spring constant and relatively clean clearance gaps). Theoretical results for sensor differential capacitance change as a function of sensor shuttle displacement showed that for the entire range of expected sensor shuttle displacements, the sensor differential change in capacitance was within the capabilities of MS3110 circuit. The MS3110 circuitry was capable of measuring capacitance changes down to 4.0 aF/rtHz, with an adjustable bandwidth of 0.5-8.0 kHz.

Figure 4 presents the shuttle displacement versus voltage bias for all the sensors on Chip 4. These results showed that the required bias voltage range, for the electrostatic actuation testing, was 10-30 Vdc for sensors A-E and as high as 50 Vdc (or more) to deflect the shuttle at least 0.1 μm for sensors F-G. The main reason for this large difference in required biasing voltage for sensors A-E and F-G is because sensors F-G have spring constants that are an order of magnitude larger.

IV. Breadboard Sensor Cold Flow Testing

The objectives of the MEMS shear stress cold flow testing were: (a) to test the sensor in a well defined flowfield and to obtain shear stress versus air mass flow rate experimental

data (and compare with theory); and (b) to assess sensor performance using open loop electronics.

The sensor was tested by introducing it into a well defined flow-field for which analytical solutions or well established empirical correlations are known. This meant providing a fully developed, turbulent flow-field in a pipe, which required a duct with a length of about 80-100D's, where 'D' was the duct diameter. The flowfield was also tailored to provide sufficient shear stress to move the sensor's sensing element and allow for measurable differential capacitance measurements.

A. Pipe Flow Theory

Prandtl's universal law of friction¹⁵, was utilized to obtain shear stress versus fluid bulk velocity and hence mass flow rate.

A theoretical relationship between fluid mass flow rate and shear stress was obtained. During the cold flow experiments, COTS electronics (MS3110 Chip, Irvine Sensors Corporation)¹¹ were used to measure the differential capacitance between the MEMS sensor shuttle fingers and the stationary electrodes.

By knowing the pressure drop along the square duct, one can then readily calculate the experimental shear stress along the wall, for incompressible, steady, fully developed flow as:¹⁶

$$\tau = \frac{-R}{2} \frac{dP}{dx} = -\frac{R}{2} \frac{\Delta P}{\Delta x} \quad (1)$$

where 'R' is the duct radius (based on hydraulic diameter) and dP/dx is the experimentally measured pressure drop along the duct, determined from seven wall pressure measurements made at 127.5", 89.5", 51.5", 13.5", 4.5" and 3.5" upstream of the MEMS shear stress sensor and 3.0" downstream of the

MEMS shear stress sensor centerline. Shear stress and V_{out} (~ shear stress) were experimentally determined as a function of air mass flow rate.

B. Cold Flow Experiment Set-up

Figure 3 shows the MEMS shear stress sensor calibration set-up. Facility main air was loaded at a given pressure (for a desired air mass flow rate) and flowed through a 0.302" diameter venturi, used to measure flow rate. Air then flowed through a 2" flexible hose which was secured to the rig and connected to the inlet of the 2" x 2" OD square, 165" long duct. Air flowed through the duct into the test section where the MEMS shear stress sensor was housed. Along the duct, there were seven static wall pressure measurements being made with a Netscanner. The cut-out in the duct test section piece, used to accommodate the MEMS sensor & packaging, was about 1.0", for a 1.5" ID duct.

Prior to testing the following pre-test procedures were implemented to ensure sensor functionality: (1) verify MS3110 board/chip settings (trim settings for differential capacitance range); (2) using a microscope inspect sensor wirebond integrity/status & take photos; (3) measure each sensor's resistance & capacitance between +/-Gnd, -/Gnd, and +/- contact pads.

When a test began, the facility data system started acquiring air mass flow rate, venturi pressures, temperatures and duct wall static pressure data. Several seconds later, the MEMS sensor data system was triggered via a remote trigger located in the control room. The sensor computer, once triggered, began acquiring the MEMS shear stress differential capacitance signal (proportional to the shear stress level), via the MS3110 board,¹¹ in the form of a voltage, V_{out}. About 1-3 seconds later, a synchronization signal was sent, from

the control room, to both the facility and sensor computers. This signal provided a marker that allowed both computers to become synchronized since the sensor computer acquired data at ~ 1 kHz, while the facility computer acquired data at ~ 4 Hz.

During the test, the air mass flow rate was varied, in stepwise fashion, from a low value to the maximum flow rate for choked flow (which was about 2 pps, for this duct geometry). For each successive step, the mass flow rate was allowed to reach steady-state. After about two minutes of testing, the data acquisition was terminated and the test was complete.

C. Cold Flow Tests Results/Analysis

Chip 4 (our best chip in terms of sensor potential performance/operation) was diced into two smaller chips, chips 4R and 4L. During electrostatic actuation tests chip 4 was found to have several sensors with bowed fingers, as shown in Figure 5. Nonetheless, it was decided to proceed with testing chip 4R as is in the wind tunnel.

The experimental shear stress was evaluated using Eqn. (1) and the differential pressure values at seven static wall pressure locations along the duct, hence 6 values of experimental shear stress were calculated at various times, Figure 6. The experimentally determined shear stress shows good comparison with the theoretical value. Figure 7 shows the Mach # and Reynolds # generated in the duct during cold flow calibration of the breadboard sensor. During steady state, the Mach # was calculated to be between 0.7-0.8 (depending on the characteristic length scale) at a Reynolds number of about 6.8×10^5 . Figure 7 also presents the MEMS shear stress sensor voltage output (from the MS3110 circuit), which is proportional to shear stress, versus time. The sensor did not begin to sense shear

stress until about 120 m/s flow or about 35 Pa of shear stress. This could be due to the fact that the sensor's shuttle fingers, as shown in Figure 5, were curled down, thus generating an immeasurable friction force. The sensor signal topped out at about 230 m/s or about 100 Pa, at which point it is believed the sensor fingers were overextended and perhaps failed. These tests served to verify the breadboard sensor design and operation, however several issues were also raised, as discussed in the next section.

V. Brassboard Sensor Design

A. Lessons Learned

In order to improve the brassboard shear stress sensor design for Phase II, our team first reviewed the Phase I breadboard sensor development effort, from sensor fabrication, handling and testing, to sensor performance prediction and potential shortfalls. This review resulted in the following compilation of the *main* technical issues and areas of improvement of the breadboard shear stress sensor: (1) out-of-plane stresses (due to residual stresses/thermal expansion, normal forces, etc) lead to fingers/electrodes curling, Figure 5; (2) the breadboard sensor design made it difficult to simultaneously actuate the sensor and sense the differential capacitance change, δC ; (3) appearance of stringers, the MEMS equivalent of "burrs" on the macro-scale level, lead to fused shuttle fingers, which subsequently prevented the sensor shuttle and fingers from becoming fully released and therefore from moving; and (4) anchor pads/finger misalignment, which also decreases sensor mobility.

Out-of-plane stresses can be minimized by decreasing the finger/electrode length L_f , thus alleviating finger deflection due to a normal force (eg. residual stresses, normal pressure load, and thermal expansion). Increasing the

finger/electrode width 'b', and height 'h', would increase its moment of inertia, also mitigating large finger deflections and the deleterious affects of out-of-plane stresses.

The breadboard sensor, with three contact pads ('+', '-', and 'ground'), made it difficult to simultaneously actuate the sensor and sense its differential capacitance change, δC . The solution to this would be to add additional front and back side contact pads, and with appropriately designed circuit paths, this would allow electrostatic actuation of the sensor with one set of pads and simultaneous measurement of the sensor's δC with another separate set of pads.

Appearance of stringers and anchor pad/finger misalignment can be mitigated, if not eliminated, through application of state-of-the-art SiC micro-fabrication techniques,¹³ which have improved since the breadboard sensor was first designed.

It should also be noted that because the breadboard sensors were not fully released (due to stringers, etc) they required high bias voltages (during electrical characterization tests) to initiate motion, which at times was actually out-of-plane motion.

B. Brassboard Sensor Requirements

Based on the lessons learned from the Phase I breadboard sensor, a set of design requirements were developed to guide the brassboard sensor design. The main requirements were: (1) high temperature capability (1500 °C); (2) test duration time of 30 seconds in an aeropropulsion wind tunnel; (3) 100 ms sensor response time; (4) maximum of 100V for sensor voltage bias; (5) sensor resolution of 10 Pa; and (6) 0-5000 Pa shear stress range.

C. Brassboard Sensor Operation

The brassboard sensor theory of operation is the same as the breadboard sensor (see Sec. III.B), i.e. differential capacitive sensing, except now closed loop feedback control will play an integral role in extending the dynamic measuring range of the sensor. The feedback control loop electronics are presently being designed.

D. Brassboard Sensor Design/Analysis

The MUSiC fabrication process used in Phase 1 to manufacture the breadboard sensor led to large residual stress gradients, some misalignment between structural layers, as well as increased feature size/ decreased gap. It should be noted that at the time of the breadboard sensor fabrication, the MUSiC process was relatively new. These fabrication issues adversely affected sensor performance often rendering the sensors completely immobile and inoperable. Phase II brassboard design analysis therefore began with the goal of minimizing any fabrication limitations or large structural deflections on sensor performance.

In taking this approach, a single layer device (Figure 8), in contrast with the multiple layer breadboard design (Figure 2), was chosen for the brassboard device.. The brassboard sensors require only one device layer to be operational, with different sets of electrodes on either side of the shuttle. This also helps in significantly decreasing the time and cost required for device fabrication.

Various parameters were analyzed during the brassboard design analysis:

- two different types of springs: folded springs and tensile beam springs, Figure 9;
- 3 pad (Figure 10b) versus 4 pad layout (Figure 10a);

- parallel versus perpendicular finger (Figure 8) arrangement;
- feature size, i.e. 4 versus 8 μm thick structures;
- 2 μm x 2 μm (finger width x finger gap) and 3 μm x 3 μm ;
- number of electrodes/fingers, N_f and finger length;
- shuttle length to width ratio, i.e shuttle aspect ratio.

Two types of finger layouts were considered: parallel and perpendicular. In the perpendicular layout, the fingers are perpendicular to the flow (Figure 8), and in the parallel layout, they are parallel to the flow. Using a perpendicular layout over a parallel layout is very beneficial because it provides higher sensitivity and larger electrostatic forces, for a given shuttle deflection (due to shear). Parallel designs have the benefit of behaving more “linearly” and are typically used as MEMS actuators, although they do not give very large electrostatic forces. The sensor design requirements stipulate that the majority of the devices were fabricated with perpendicular fingers.

Folded-spring designs were modeled using ANSYS by assuming a steady-state temperature gradient throughout the shuttle thickness. A temperature gradient and coefficient of thermal expansion were chosen to produce a residual stress of 50MPa/ μm , a typical value for MEMS devices, incurred during the fabrication process. The main parameters that were varied were: (1) the number of fingers, N_f (this dictates the shuttle length); (2) the length of the fingers L_f and springs L ; and (3) the shuttle width, w . Structural analysis focused on the deflection at the center of the shuttle and at the tips of the fingers. Because the entire shuttle bends

similar to a paraboloid, the center of the shuttle may move vertically up from the initial plane, while the finger tips may bend down. The initial thought was that the folded springs would act as torsional springs, attached to a rigid plate, rotating from the applied moment. ANSYS results showed that long shuttles were susceptible to bending, because the folded springs themselves would bend rather than rotate and the shuttles were not rigid. ANSYS structural results showed that deflections were much lower for aspect ratios (L/W) in the range of 3-5, Figure 11.

The tensile spring designs were not modeled, however it is estimated that for a given shuttle length, sensor designs with tensile springs will deflect less than the folded spring. ANSYS analysis also verified spring stiffness in the x, y, and z, directions, and showed that device layer thickness has minimal effect on the device deflection. This last result is important, as a larger device layer (i.e. 8 μm) increases sensor sensitivity and shear stress range, although increases the risks associated with fabrication errors and stress gradients (50 MPa/thickness). It was decided to fabricate wafers with 4 μm device layer with an underlying 4 μm anchor layer, which will provide adequate spacing for potential structural deflections, with no obstructions.

Both stationary and moving fingers are at risk for out-of-plane bending from stress gradients, and for bending in the flow direction from electrostatic forces. This is because the high-aspect ratio fingers are of comparable dimensions to the springs, which are designed to bend. As electrostatic forces are felt on both the stationary and moving fingers, fingers are pulled towards each other from both directions. Analysis showed that fingers 100 μm or longer are very sensitive to this bending. Therefore anchor pads are placed

underneath all stationary fingers 100 μm or longer.

Fabrication of the brassboard sensors will be conducted at CWRU, where Prof. Mehregany's laboratory and facilities have developed SiC microfabrication techniques¹³ over the past several years, which can handle 2 μm feature dimensions and 2 μm gaps. Due to fabrication issues, breadboard sensor designs typically had a finger width increase from 1 μm –2 μm for 2.5 μm fingers, sometimes leading to complete closure of finger gaps. To minimize the chances of this finger gap closure occurring designs are also included for 3 μm features and 3 μm gaps. Fabrication of finger widths exactly as designed is not feasible; however finger width is critical to sensor performance. The smallest features available from typical mask-making procedures are 2 μm with a tolerance of +/- 0.5 μm , which is unacceptably risky. Therefore, a more expensive electron beam lithography process was utilized to fabricate the masks with a tolerance of +/- 0.1 μm .

Misalignment errors result from two consecutive layers not being perfectly deposited on top of each other, or not being fabricated exactly as designed. Breadboard sensors had misalignments as large as 1.5 μm , which can, at best, limit the sensor's operational range or at worst fix the shuttle and stationary electrode fingers together. In the brassboard design, the anchor layer is constructed so that a layer misalignment of up to 3 μm in any direction will not destroy the devices. Other layers have much larger features (at least 100 μm) with large overlap between layers, so that sensor performance will not be sensitive to feature resolution and misalignment errors.

Phase I experience showed it was very difficult, with the breadboard design, to measure differential capacitance while simultaneously applying a large bias voltage across the same electrodes. In fact, the MS3110 circuitry¹¹ could not handle voltages > 5V. Previous MEMS devices using electrostatic actuation and capacitive sensing used a single set of electrodes for both signals, multiplexing a high frequency low voltage signal for sensing, and a low frequency high voltage signal for actuation. Other designs have separate fingers for actuation and sensing, using a high-frequency AC signal for sensing and a separate DC bias for actuation. Our brassboard sensor designs will have a combination of 3-Pad designs (Figure 10b, bidirectional shear stress sensing which requires frequency multiplexing) and 4-Pad designs (Figure 10a, unidirectional shear stress sensing, which requires more electrical connections).

VI. Future Plans

In addition to our work on designing, fabricating and testing a MEMS shear stress sensor, an on-going, parallel research effort pertaining to high temperature electrical connections and SiC deep etching techniques is being conducted by our team at the University of Sherbrooke.

At the present time the MEMS shear stress brassboard sensor masks have been designed and are awaiting fabrication. The sensors will be fabricated at Case Western Reserve University, under the guidance of Prof. Mehregany, with completion expected early Fall, 2006.

Initial device inspection and electrical characterization will be performed in the Microsystems Laboratory at Columbia University in order to validate the dimensions and basic functionality of the sensors. The

mechanics of the device will be characterized through electrostatic actuation and dynamic response testing. Final packaging of the sensors will be conducted at ATK GASL, early Fall 2006.

Breadboard closed loop electronics with off-the-shelf integrated circuitry for differential capacitance measurement and feedback control will be used initially, but can eventually be miniaturized at the chip scale.

Previous sensor designs such as accelerometers and shear stress sensors have built their own circuits for both sensing and feedback, utilizing both analog and digital designs. Attempts will be made to use the MS3110 IC (Irvine Sensors, Inc.) for capacitive sensing, and a PICmicro® Microcontroller (Microchip, Inc.) to implement the feedback control. The PICmicro® is an embedded microcontroller which can be programmed in both Assembly and C, and can run instructions up to 40MHz. Other circuits will also be investigated and tested to determine the best operation.

Flow testing will then be conducted in the low speed wind tunnel and Mach 2 blowdown supersonic tunnel at Columbia University in order to develop necessary instrumentation and to calibrate device operation. Upon satisfactory performance, select sensors will be packaged for testing in the high speed tunnels at the Test and Evaluation Laboratory at ATK GASL and their performance evaluated.

The Test and Evaluation Laboratory has six high-temperature aeropropulsion wind tunnels capable of achieving total temperatures up to 5600 °F and total pressures up to 1800 psi. Experiments range from combustor testing (Legs 1 and 2), to materials testing (Leg 3)

and scale model testing of freejet engines (Legs 4-6).

VII. Summary and Conclusions

In this paper, we present our efforts over the past year and half to design, develop, fabricate and test a silicon carbide (SiC) MEMS shear stress sensor for hypersonic aeropropulsion test and evaluation applications. During this initial research and development work, two generations of MEMS-based direct shear sensors were designed, fabricated and tested. The MEMS sensors consists of a silicon carbide, surface micromachined, freely-suspended sensing element, whose motion is sensed capacitively and negated with force feedback control to achieve the large shear stress range. Brassboard sensors are currently under fabrication and testing plans were presented. Such shear measurements would: (1) allow for the calibration of computer code shear stress calculations; (2) help identify when and where flow separation and boundary layer transition occurs in the engine flow path; and (3) allow for direct measurement of vehicle component drag.

VIII. Acknowledgements

The authors would like to thank: (1) the Test Resource Management Center (TRMC) Test and Evaluation/Science and Technology (T&E/S&T) Program for their support. This work is funded through Arnold Engineering Development Center, Arnold Air Force Base, TN; (2) Bob Stark and Walter Khan of the ME Department Machine Shop at Columbia University for fabricating the cold flow test hardware; (3) Prof. Mehregany of Case Western Reserve University; and (4) Ralph Woelfel, principal scientist at ATK GASL, for conducting the ANSYS structural analysis for the brassboard sensor.

	Sensors						
	Primary		Off-Design				
	A	B	C	D	E	F	G
Dimensions							
a (μm)	2.5	2.5	4.0	2.5	4.0	4.0	4.0
b (μm)	4.0	8.0	4.0	8.0	4.0	8.0	8.0
L (μm)	190.0	190.0	190.0	190.0	190.0	100.0	100.0
Lf (μm)	115.0	115.0	115.0	115.0	115.0	115.0	115.0
r (μm x μm)	92 x 92	87 x 87	51 x 51	275 x 275	163 x 163	445 x 445	140 x 140
Nf	52.0	46.0	42.0	46.0	42.0	34.0	34.0
Ranges							
τ_{min} (Pa)	10	100	100	10	10	90	900
τ_{max} (Pa)	10000	10000	10000	1000	1000	110	1100
							96.43

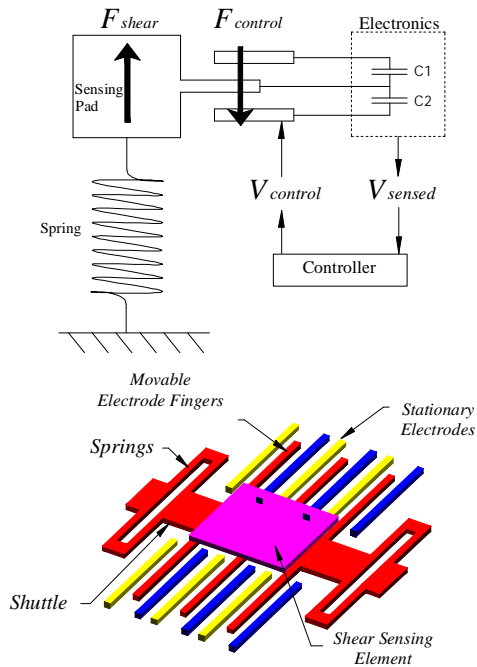


Figure 1: MEMS shear stress sensor operating principle and configuration.

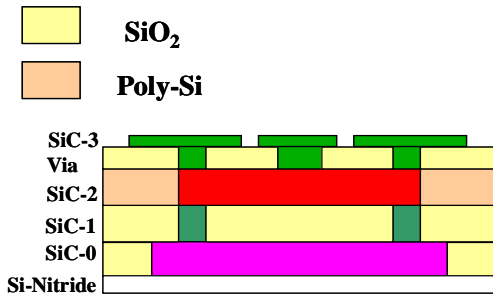


Figure 2: Schematic of the various layers of the MEMS shear stress breadboard sensor fabricated using the MUSiC process.

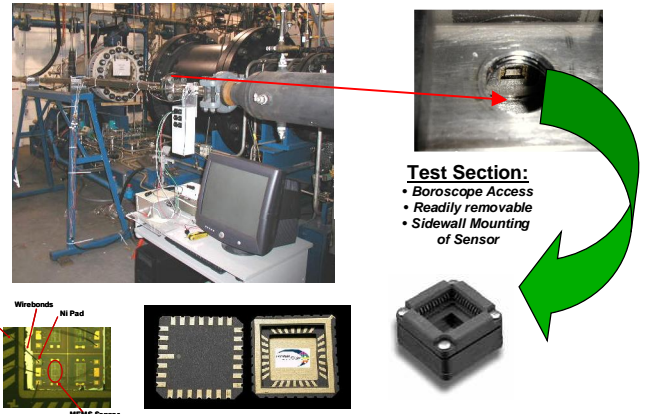


Figure 3: Going clockwise: Cold flow test set-up; boroscope access view port showing breadboard sensor flush mounted to duct wall; COTS mount; LCC package; close up photo of wirebonds connecting sensor pads to LCC terminals, for signal transmission to data system.

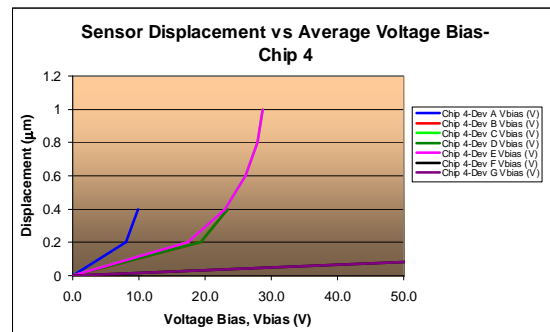


Figure 4: Sensor shuttle displacement as a function of voltage bias, for all the sensors on Chip 4.

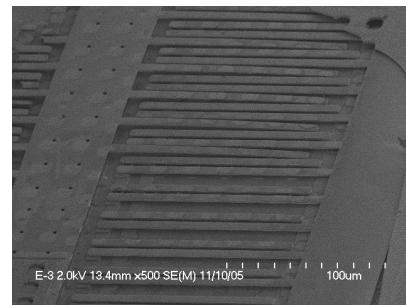


Figure 5: SEM photograph of a breadboard sensor from Chip 4, showing the effects of large residual stresses on the bending/curling of the shuttle fingers.

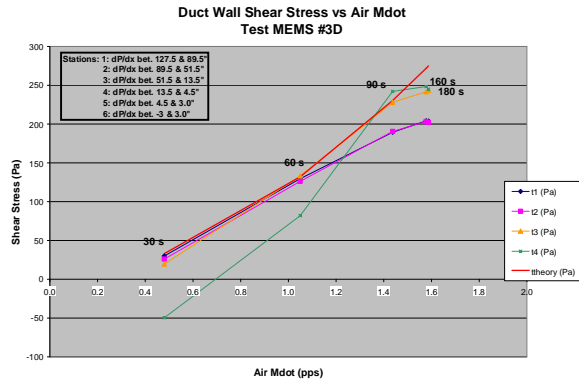


Figure 6 Shown above is a plot of experimental data for shear stress versus air mass flow rate during cold flow testing of the breadboard sensor.

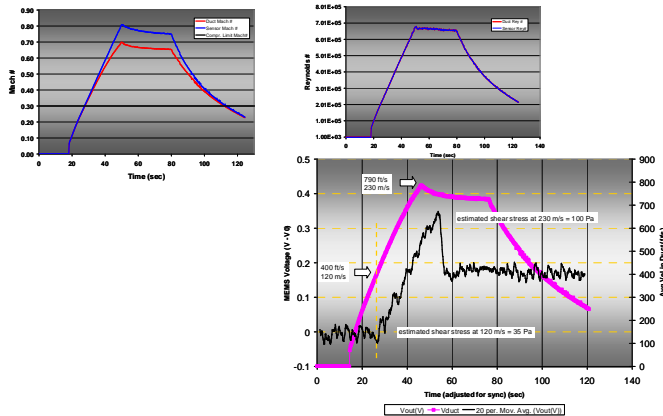


Figure 7 Mach #, Reynolds # and breadboard sensor voltage output (proportional to shear stress) as a function of cold flow test time.

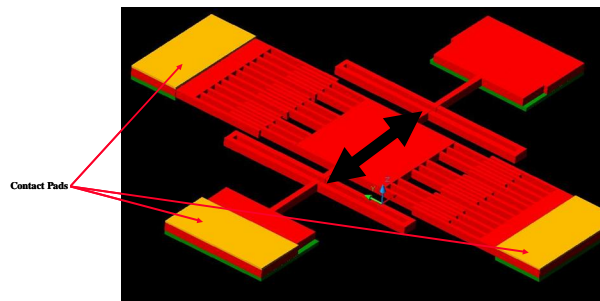


Figure 8 Schematic of the single layer brassboard sensor, with 3 Pads and perpendicular finger configuration.

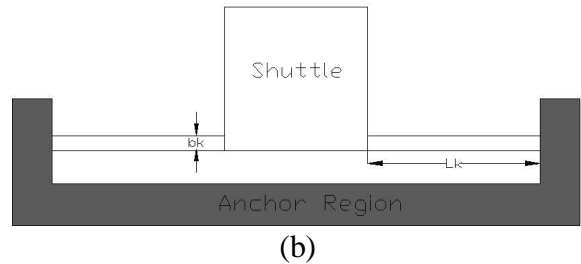
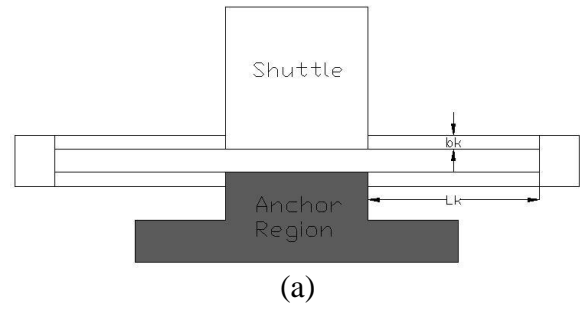


Figure 9 (a) Folded versus (b) tensile beam spring components of the shear sensor.

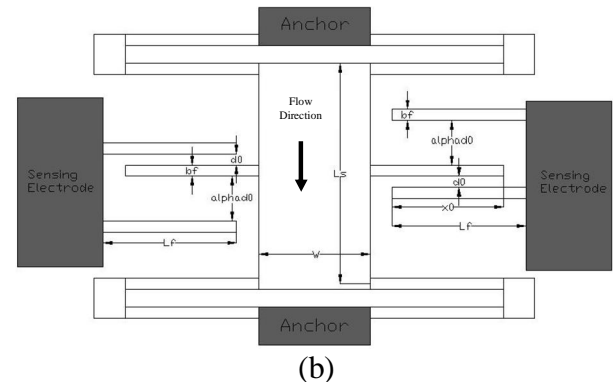
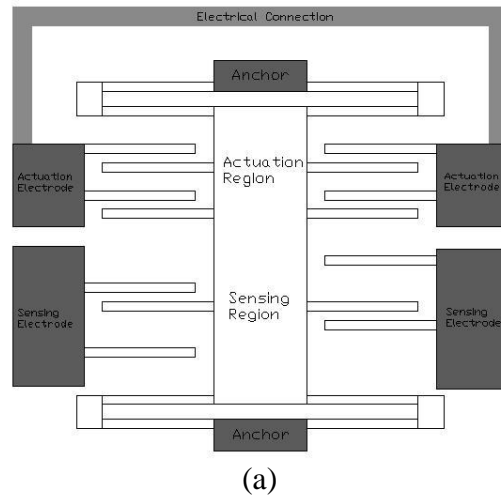


Figure 10 MEMS brassboard sensor, single layer designs with: (a) 4 pad configuration; and (b) 3 pad configuration

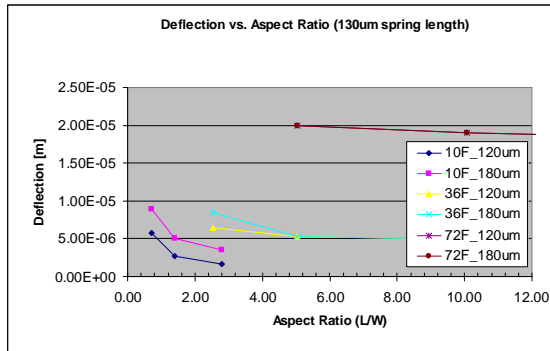


Figure 11 Brassboard sensor device deflection as a function of shuttle aspect ratio for various finger and spring lengths.

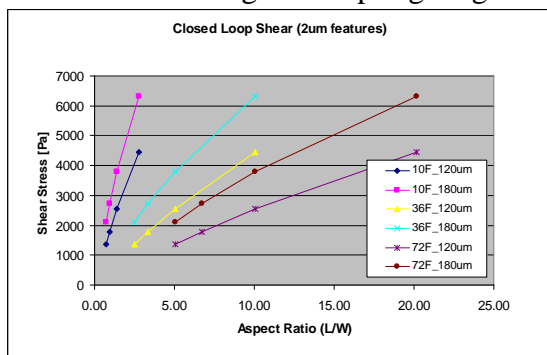


Figure 12 Brassboard sensor device shear stress (closed loop) as a function of shuttle aspect ratio for various finger and spring lengths.

IX. References

- ¹McCarthy, M., Frechette, L.G., Modi, V., and Tiliakos, N., "Initial Development of a Wall Shear Stress Sensor for Propulsion Applications," presented at the Propulsion Measurement Sensor Development Workshop, May 12-13, 2003, Huntsville, AL..
- ²Haritonidis, J.H., "The Measurement of Wall Shear Stress", Advances in Fluid Mechanics Measurements, Springer-Verlag, pp. 229-261.
- ³Dhawan, S., "Direct Measurements of Skin Friction", NACA TN 2567, 1953.
- ⁴Mabey, D.G., Gaudet, L., "Some Performance of Small Skin Friction Balances at Supersonic Speeds," *J. Aircraft*, Vol. 12., pp. 819-825.

⁵Preston, J.H., "The Determination of Turbulent Skin Friction by Means of Pitot Tubes," *J. R. Aero. Soc.*, Vol. 58., pp. 109-121.

⁶Hool, J.H., "Measurement of Skin Friction Using Surface Tubes," *Aircraft Eng.*, Vol. 28., pp. 52.

⁷Rubessin, M.W., Okuno, A.F., Mateer, G.G., and Brosh, A., "A Hot-Wire Surface Gage for Skin Friction and Separation Detection Measurements," NASA TM X-62, pp. 465.

⁸Papen, T.V., Ngo, H.D., Obermeier, E., Schober, M., Pirskawetz, S., and Fernholz, H.H., "A MEMS Surface Fence Sensor for Wall Shear Stress Measurement in Turbulent Flow Areas", Technische Universitat Berlin, papen@mat.ee.tu-berlin.de

⁹Liu, C., Tai, Y.C., Huang, J.B., and Ho, C.M., "Surface Micromachined Thermal Shear Stress Sensor".

¹⁰Zhe, J., Farmer, K.R., and Modi, V., "A MEMS Device for Measurement of Skin Friction with Capacitive Sensing," Dept. of Mechanical Engineering, Columbia University, N.Y., and Microelectronics Research Center, NJIT, Newark, N.J.

¹¹Irvine Sensors Corp. literature on MS3110 Universal Capacitive Readout IC.

¹²Raizer, Y.P., Gas Discharge Physics, Springer-Verlag, 1991.

¹³Private communication with Prof. Mehregany, Case Western Reserve University (CWRU).

¹⁴J.M. Melzak, A. Leppart, S. Rajgopal, and K.M. Moses, "MUSiC - an Enabling Microfabrication Process for MEMS," Proc. of Commercialization of Micro Systems Conference, Ypsilanti, MI, September 8-12, 2002, p. 515.

¹⁵Schlichting, H., Boundary-Layer Theory, McGraw-Hill Publishing, 7th Edition, 1987.

¹⁶Fox, R.W., and McDonald, A.T., Introduction to Fluid Mechanics, 3rd Edition, John Wiley & Sons, 1985.